

# **Fan-Stage Broadband Interaction Noise Trends**

Nuo Li\*, Berkely Wachtmann<sup>†</sup>, Tyler Ramsarran<sup>†</sup> Boston University, Boston, MA, 02215, U.S.A.

Julian Winkler<sup>‡</sup>, C. Aaron Reimann<sup>§</sup>, Dmytro Voytovych<sup>¶</sup>, Jeff Mendoza<sup>∥</sup> *Raytheon Technologies Research Center, East Hartford, CT, 06108, U.S.A.* 

Sheryl M. Grace\*\*

Boston University, Boston, MA, 02215, U.S.A.

A large contributor to modern turbofan engine noise is broadband fan-stage interaction noise. Previously, a low-order method for predicting the broadband interaction noise downstream of the fan exit guide vane was developed and validated against NASA's experimental results for the scaled fan Source Diagnostic Test (SDT). In this paper, predictions obtained with this low-order method are shown for the newer ACAT1 scaled fan experiment. As with the SDT results, the trend with fan speed is shown to be predicted well. The low-order method is then used to investigate the effect of fan geometry, fan speed, fan mass flow rate and interstage gap on the broadband noise in a fan stage. The strongest influencing parameters will be highlighted.

## I. Introduction

As fan size and bypass ratio increase in turbofan engines, so does the contribution of fan-stage noise to overall engine noise. Broadband noise due to the interaction of the fan wake with the fan exit guide vane (FEGV) is now a dominant noise source. Recently, low-order methods for predicting the broadband interaction noise in a fan stage has enabled the study of fan-stage design on noise. One such low-order method has been described previously in Ref. [1] and is briefly reviewed in Section III. In the present application of the method, the fan wake upstream of the FEGV is determined using rotor alone Reynolds Averaged Navier Stokes (RANS) simulations. The method was validated against data from NASA's Source Diagnostic Test (SDT) and trends with both fan speed and FEGV geometry were captured. In this paper, the validation is extended to the AneCom AeroTest (ACAT1) scaled rig and again trends are well predicted as shown in Section IV. This paper then uses the low-order capability to explore the broadband noise created by different fan geometries, fan speeds, fan mass flow rate, and interstage gap extents. Section IV describes the noise trends based on the geometry and flow parameter variations.

### II. Background

The paper by Guérin [2] gives an excellent overview of methods developed over the last decade for predicting broadband interaction fan stage noise. The low-order methods described in that paper all focus on the FEGV and its response to the turbulence in the fan wake. There are differences between how the FEGV response is calculated but most convert the 3D FEGV into 2D strips and perform a cascade response calculation in the frequency domain [1, 3–5]. Many approximate the 2D FEGV section shape as a flat plate but there are some that model the exact shape such as Blázquez and Corral [5]. Finally, there are two main methods used to couple the FEGV response to the noise produced: a rectilinear propagation model and an annular propagation model. Over the years, no method has stood out as the most accurate for any given validation case and most have been shown to produce reasonable trends for the validation cases.

The research on broadband interaction noise modeling has heavily focused on method development, verification and validation; and, the developers of the methods have not been fan-stage designers. Therefore, the literature includes many

<sup>\*</sup>Graduate Student, Mechanical Engineering Department, AIAA Student Member.

<sup>&</sup>lt;sup>†</sup>Undergraduate Student, Mechanical Engineering Department, AIAA Student Member.

<sup>&</sup>lt;sup>‡</sup>Sr. Principal Engineer, Acoustics, Aerothermal & Intelligent Systems Department, AIAA Senior Member.

<sup>§</sup>Sr. Manager, Acoustics, Aerothermal & Intelligent Systems Department, AIAA Senior Member.

<sup>¶</sup>Principal Engineer, Aerodynamics, Aerothermal & Intelligent Systems Department.

Technical Fellow, Acoustics, Aerothermal & Intelligent Systems Department, AIAA Associate Fellow.

<sup>\*\*</sup>Associate Professor, Mechanical Engineering Department, AIAA Associate Fellow.

instances of simulations related to the specific geometries and conditions of the SDT and ACAT1 validation tests. These rig tests provided noise measurements from several rotor speeds and either different FEGVs (SDT) [6] or different placement of the FEGV (ACAT1) [7]. Still there are a few trends that have yet to be demonstrated as well as modeled by the low-order methods. One example is the lack of influence of fan tip clearance on the broadband interaction noise. It is also of interest to move beyond the application of the low-order method to these validation cases. The confidence that has been built through the verification and validation stage now prompts the use of the methods to gain insight into the impact of fan stage design and operating point differences on the broadband noise. The work described in this paper is a start in this direction.

### III. Method

The fan exit-guide vane response and acoustic propagation are formulated based on the Linearized Euler Equations valid for inviscid flows and small perturbations. The calculations are carried out in the wave-number, frequency domain. The FEGVs are modeled using strip theory enabling 2D analysis at each strip. The section geometry of each strip is approximated as flat with a specified stagger angle. For the cascade aerodynamic response, it is assumed that the mean inflow to the vanes is perfectly aligned in the chordwise direction at each radial strip. The turbulence in the fan wake is represented in the frequency-wave number domain via the Liepmann turbulence spectrum. The assumption of linearity for the unsteady aerodynamics allows one to consider the turbulence as a series of individual frequency, wave-number disturbances called gusts. The two-dimensional cascade response (i.e. the unsteady pressure jump for a flat-plate cascade) to a gust is computed using an integral equation method derived in the book by Goldstein [8] and the technical report of Ventres [9] with the extension to three-dimensional gusts being described by Hamad and Atassi [10]. The unsteady lift response, L', associated with the flat-plate cascade-gust interaction for a specified frequency and wave number vector can be calculated by integrating the unsteady pressure  $\Delta \hat{p}$  along the chord.

The acoustic pressure as a series of modes at a given downstream duct location is then computed using a Green's function transfer method based on annular duct acoustic pressure modes. Once the pressure in the duct downstream of the FEGV is known, it is used to determine the acoustic power. Details of the method have been provided previously [11].

In order to apply this method, the mean flow and turbulence upstream of the FEGV must be known. For results shown in this paper, the turbulence parameters are derived from Reynolds Averaged Navier Stokes (RANS) computations. For all of the SDT related cases, the simulations were performed using a multi-block structured code (UTCFD) that solves the compressible unsteady Reynolds-averaged Navier–Stokes equations (URANS) for an ideal gas. The code uses the Lax-Wendroff multiple grid scheme of Ni [12], centered second-order spatial differencing with second-order and fourth-order smoothing. Turbulence is modeled using the k- $\omega$ -model of Wilcox [13]. The solver has been extensively validated for numerous turbomachinery applications, including acoustic studies. For recent application of the present CFD code to turbofan noise predictions see Winkler et al. [14, 15] and Prasad et al. [16].

For the current CFD simulations, the fan alone is simulated as a single sector with periodic boundary conditions, and the governing equations are solved in a steady state fashion in the rotating frame of reference. The inlet and outlet conditions are steady 2D non-reflecting characteristic boundary conditions, based on Giles [17]. Initial total pressure and temperature profiles are specified at the domain inlet, and the desired target mass-flow rate is specified at the domain outlet, together with a radial equilibrium assumption of the flow. All simulations are run until all monitor points reach a converged value. The computational grid consists of 145 radial points and 25 points in the tip gap, where the nominal tip gap size is 0.02". The total grid count for the single rotor passage is approximately 7.2 million. While the RANS, fan-alone, computations are faster than URANS or LES, the simulations still require roughly 25 hours per case when running on a single core. The wall clock time can be reduced of course by using multiple cores.

When using the RANS data, the turbulence intensity is computed as  $\sqrt{2/3k}$  where k is the turbulence model parameter representing the turbulent kinetic energy. The other required turbulence parameter is the length scale. There are two length scales that appear in the Green's method formulation: the longitudinal length scale in the streamwise direction  $\Lambda_s$  and the lateral length scale in the radial direction,  $\Lambda_{rad}$ . Here,  $\Lambda_s$  is computed from RANS data using Pope's [18] formula relating the turbulent kinetic energy and eddy dissipation to the length scale via  $\Lambda_s = 0.43k^{1.5}/\epsilon$  where  $\epsilon$  is the turbulence dissipation provided by the RANS turbulence model. (When a  $k - \omega$  model is used,  $\epsilon = 0.09\omega k$ ). The lateral length scale in the radial direction is assumed to be the same as the lateral length scale in any direction, so the upwash velocity component from the hotwire can be used to compute this length scale. Analysis of the hotwire data previously showed that a reasonable approximation to the lateral length scale is one half of the longitudinal length scale [19]. This relationship has been used in this work even for cases that derive their input from the experimental data.

### IV. Model behavior and validation

Before discussing new cases to which the current low-order method is applied, a review of some outcomes and dependencies of the method is provided. Motivation for providing these results is to show the predictions when Pope's model for the length scale based on RANS parameters is used and to review how model choices impact the predictions generated by this method.

#### A. SDT prediction and effect of stagger

A schematic of the SDT fan stage is presented in Fig. 1. The original baseline FEGV is shown in blue and its leading edge position is 0.56 from the rotor tip trailing edge normalized by the rotor tip radius, 11". In the SDT experiments, flow measurements were taken at this axial position. The position will be referred to as Station 2 in this paper. The red

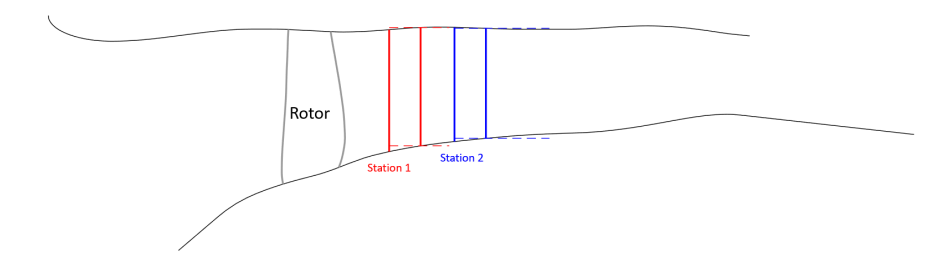


Fig. 1 Schematic of FEGV locations for SDT configuration. Red solid and red dashed: baseline vane at station 1 and assumed downstream duct geometry. Blue solid and blue dashed: baseline vane at station 2 and assumed downstream duct geometry.

FEGV shown in the figure represents a similar vane with leading edge situated close to the mid interstage gap. This vane will be discussed in Section V.C. Flow data were also recorded experimentally at its leading edge position, 0.27. This location will be referred to as Station 1. The acoustic predictions of the broadband interaction noise obtained when utilizing the experimental data at Station 2 as input to the FEGV low-order calculation were presented in Ref. [1]. In this paper, the focus is on predicting the noise based on RANS simulations of the fan wake. This was also discussed in [1], however, new RANS simulations are being used here.

The acoustic results downstream of the fan stage for the main SDT fan speed cases with the baseline vane are shown in Fig. 2. The three speed lines are namely approach (61.7%), cutback (87.5%), and takeoff (100%) and the accompanying corrected mass flow rates as reported for the full fan stage in [20] are 58.3 lbm/s, 83.91 lbm/s, 97.18 lbm/s respectively. The fan geometry for each fan speed is slightly different due to the aerodynamic structural loading. As such, the RANS was performed for the fan "hot" geometries as previously determined by researchers at NASA [6]. The sound power spectrum predicted by the low-order method is compared with the measured spectrum in Fig. 2. A bandwidth correction is applied to the predicted spectrum to allow for comparison to the experimental spectrum. The experimental data are only shown at frequencies NASA researchers determined were not contaminated by facility or equipment noise. The approach speed is slightly overpredicted while the other speeds, where they can be validated, show good agreement with experiment.

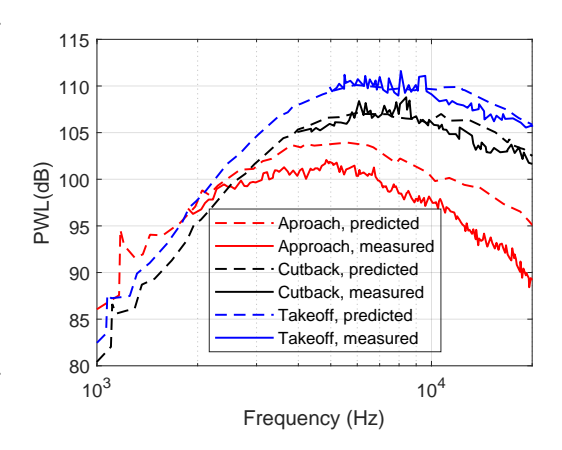


Fig. 2 PWL for SDT baseline vane predicted using the rotor alone RANS input data at 3 fan speeds.

The RANS based input used for the predictions are shown

in Fig. 3 as functions of radial location. These data have been extracted from the RANS simulation at Station 2 and are obtained by averaging in the circumferential direction over the passage. The turbulence intensity is normalized by the streamwise velocity and the turbulence length scale is normalized by the fan radius. It is observed that the flow Mach number increases with fan speed as expected. The turbulence quantities however, indicate that the approach case is quite

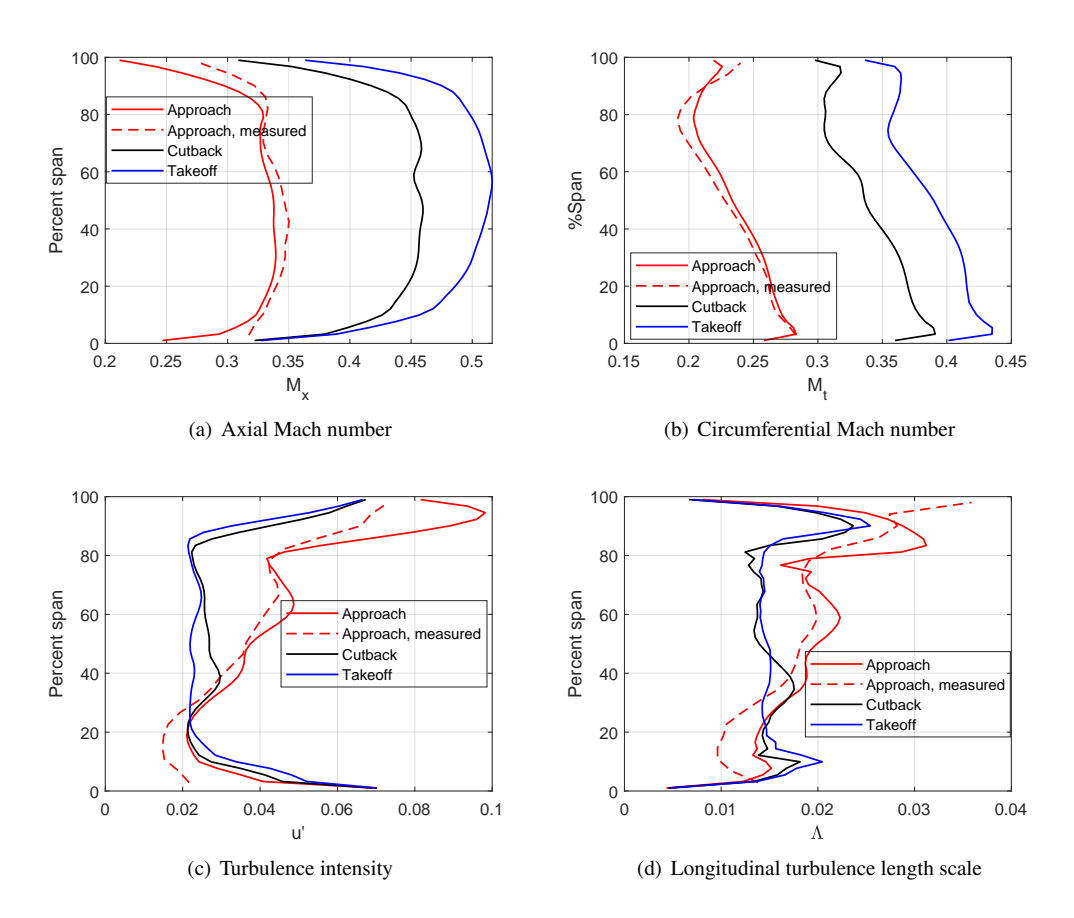


Fig. 3 Inputs for acoustic prediction from RANS simulation. Top Left: Axial Mach number. Top right: Circumferential Mach number. Bottom left: nondimensional turbulence intensity. Bottom right: nondimensional longitudinal turbulence length scale.

off design leading to greater turbulence with larger length scales in the fan wake. The hotwire measured data at the approach speed is plotted as red dashed lines and the RANS extracted input shows good agreement with the measured.

The model requires the user to specify a stagger angle for the flat plate representation of the vane section at each radial strip. Fig. 4 shows the predictions for the noise at the cutback fan speed based on 3 different vane stagger selections. The significant dependence of the result on the choice of stagger was demonstrated previously [1]. Equally important though is the fact that once a stagger selection method is fixed, the predicted noise trends with fan speed and SDT FEGV type are the same as shown by the black lines in Fig. 5. In Section V.A, the noise trend with mass flow rate is also shown to be independent of stagger selection.

### **B. ACAT1 prediction**

The low-order method used here was only validated against the SDT cases previously. The ACAT1 fan test now provides another benchmarking platform [2]. For ACAT1, the FEGV geometry information used to obtain the present results is calculated by averaging the leading edge and trailing edge stagger information given in Ref. [2]. The fan wake information required for the low-order calculation, i.e.

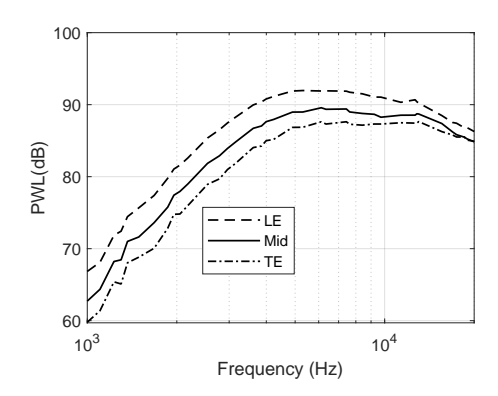


Fig. 4 Effect of stagger selection computed at the SDT cutback fan speed with the baseline vane (no bandwidth correction applied).

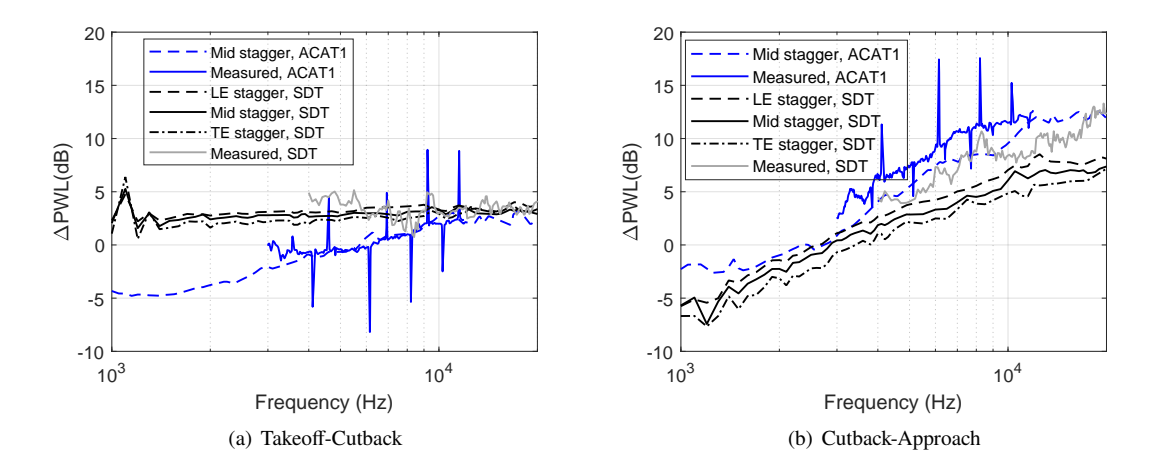


Fig. 5 Sound power difference. Left: Takeoff-cutback. Right: Cutback-approach.

mean velocity, turbulence length scale, turbulence kinetic energy as

well as the measured acoustic power for comparison are all taken from Ref. [2]. The results are shown in Fig. 6. Two predictions that are presented in Ref. [2] are also included in Fig. 6. The Hanson method [21] shown as the red dashed line and Posson method [4] shown as the red dotted line are very similar to the current method and as such these were chosen for comparison. At both approach and takeoff conditions, our prediction agrees with the Hanson method in the midfrequency range but tends towards the Posson method in the lower frequency range. A general observation is that unlike the SDT predictions which exceed the measured values at the approach speed (refer back to Fig. 2), all of these predictions are well under the measured acoustic power. The trend with fan speed for the ACAT1 is shown with the blue lines in Fig. 5. The trends are similar in nature to the SDT trends as the fan stages are similar in type. The SDT and ACAT1 results indicate that the low-order method gives a relatively higher sound power prediction for the approach speed than seen experimentally. The source of this increased level is not understood currently.

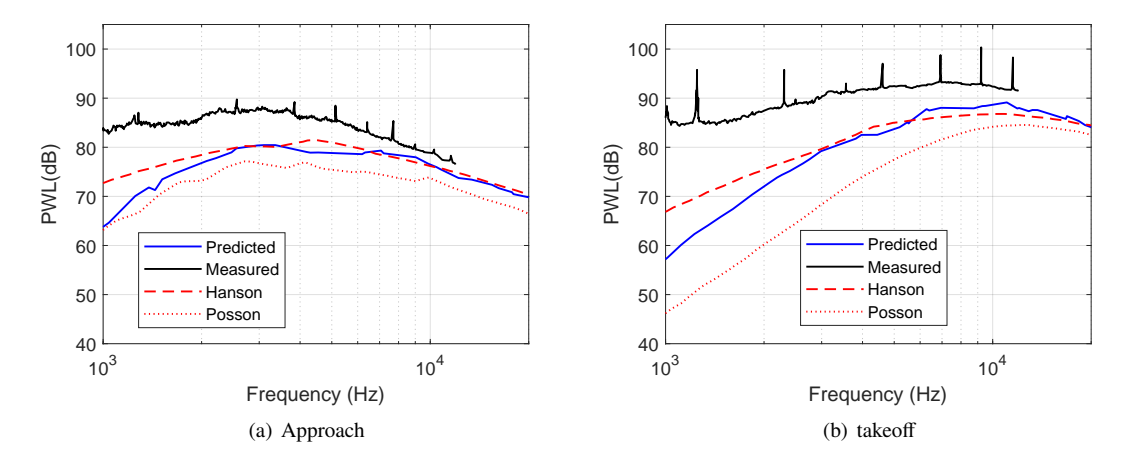
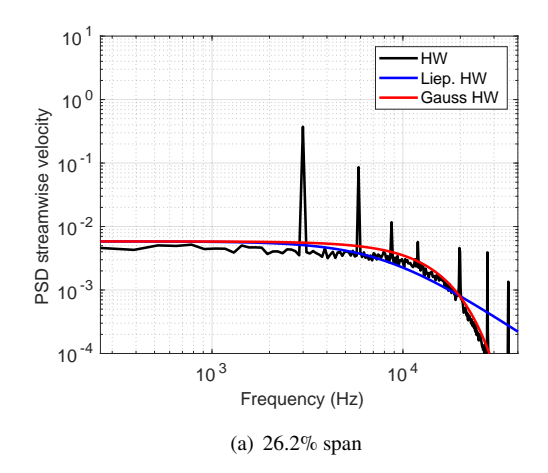


Fig. 6 Low-order downstream acoustic prediction of ACAT1 approach and takeoff cases with digitized RANS data as input. Results previously reported using Hanson and Posson low-order methods have also been digitized for comparison.

### C. Effect of spectral model

The low-order model requires an analytical description of the turbulent velocity spectrum that is informed by the turbulence intensity and turbulence length scale. As mentioned above, the Liepmann model has mainly been used.



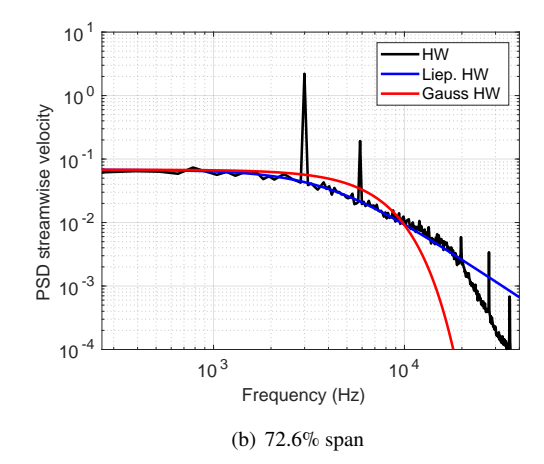


Fig. 7 Approach fan speed. Streamwise velocity spectra at Station 2. Original spectrum from data. Liepmann and Gaussian based on turbulence intensity and length scale values determined from the original data. Left: inboard. Right: outboard.

However, analysis of the velocity spectrum from the SDT experimental hotwire data indicates that near the hub, the turbulence spectrum is better fit using a Gaussian spectrum. Fig. 7 shows this. When a Gaussian spectrum is used inboard (less than 40% span) and Liepmann is used outboard, the prediction obtained between 6 and 15 kHz with the low-order model deviates slightly from the prediction using the Liepmann spectrum everywhere as shown in Fig. 8. Unfortunately, neither the SDT nor ACAT1 data allows one to discern which predicted acoustic result is correct. All that can be stated currently is that the method by which the inflow turbulence spectrum is modeled leads to slightly different outcomes. The differences are small enough that the mixed spectral model based on span location is deemed unnecessary.

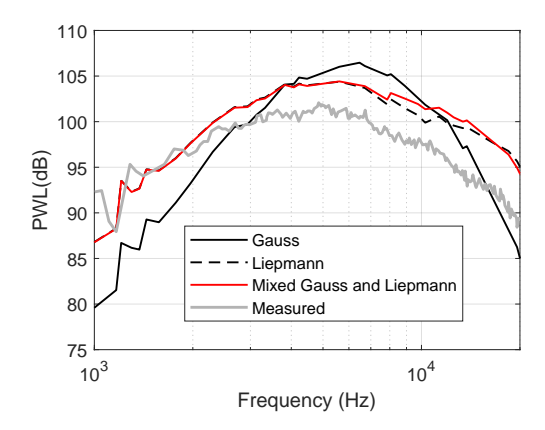


Fig. 8 Effect of using different turbulence spectrum on predicted PWL. SDT 61.7% speed and 58.3 lbm/s.

# V. Fan parameter and operating point impact

#### A. Fan speed and mass flow rate

As part of the SDT, the fan performance was measured over speeds ranging from 50%-100% design speed (12657 rpm) and over a range of mass flow rates. In this study, the fan at similar speeds and mass flow rates was simulated with RANS. Four slightly different fan geometries exist for the SDT: the cold or CAD basic geometry and then the aerodynamically deformed "hot" geometries at three fan speeds: approach, cutback and takeoff. Fig. 9 provides the performance plot for the calculations using the fan geometry based on the original CAD or the "cold" geometry.

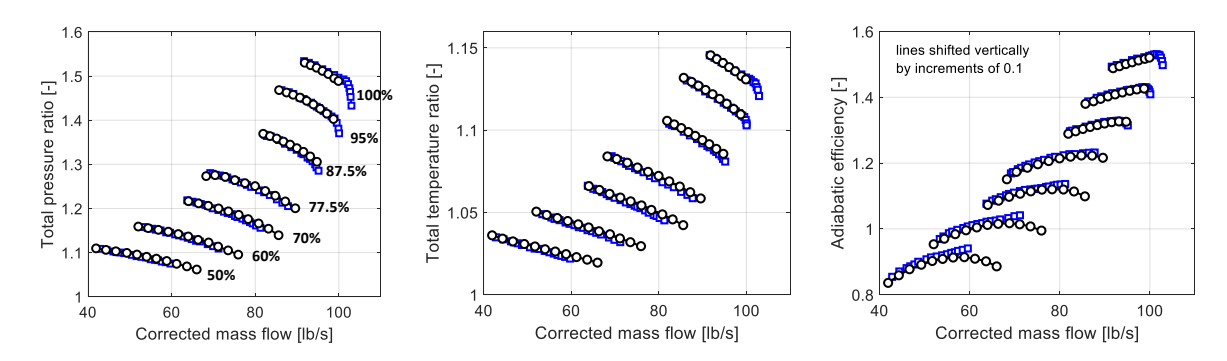


Fig. 9 Performance plot for basic SDT cold geometry. Blue – experimental data digitized from NASA TM 2013-214029 [22]. Black – CFD results.

The effect of changing mass flow rate on the noise was considered. The 87.5% speed line which corresponds to the cutback case was considered first. The fan wake parameters for the cutback hot geometry at Station 2 for 4 mass flow rates are shown in Fig. 10.

The power spectrum downstream of the baseline vane for each mass flow rate case is given in Fig. 11. The decrease in turbulence intensity with increased mass flow rate reduces the overall spectrum. The decrease in length scale tilts the spectrum such that it is lower at lower frequency and higher at higher frequency. This effect has been demonstrated previously [1, 23]. There is an increase in the streamwise Mach number (combination of axial and circumferential) with increased mass flow and this slightly increases the sound power at higher frequency. The largest contributor to the differences shown in Fig. 11 is the length scale.

In order to compare multiple cases of fan speed and mass flow simultaneously, acoustic metrics for the sound power spectrum have been devised: the maximum sound power level over the entire frequency range, and an integrated sound power:  $\overline{P} = \int_{f_1}^{f_2} P df / (f_2 - f_1)$  where  $f_1 = 600Hz$  and  $f_2 = 20,000Hz$ . The integrated sound power is then converted to decibel using  $10 \log_{10}(\overline{P}/P_0)$ .

The computed acoustic metrics for the cutback fan speed with the cutback hot fan geometry and the baseline FEGV are shown in Fig. 12. It is observed when comparing the left and right plots that both metrics give the same trend with mass flow. It is also observed, as discussed earlier, that there is very little difference in the mass flow trend obtained when using different stagger angle selections. For the leading edge stagger case, the integrated metrics predict a spread of about 3 dB over the mass flow cases considered while the trailing edge stagger gives a spread less than 2 dB.

The sound power metrics for all of the fan speeds and mass flows computed are plotted in Fig. 13. For all of the the cases, the cutback hot fan geometry has been used. The green curve corresponds to the case described above, i.e. Fig. 11. At each speedline, the integrated PWL (left) and maximum PWL (right) are similar. In terms of acoustic production, an optimal mass flow rate emerges especially at the lower fan speeds. The acoustic trend with mass flow does not mirror the total pressure ratio or efficiency. The integrated PWL values are shown as a contour map superposed on the performance map in Fig. 14. It was already discussed that as the inflow mean speed increases, it increases the noise at the high frequencies. This increase in mean inflow speed comes both from high fan speed and from higher mass flow. This explains the general increase with speed line. It also explains the right side of the curve at any speed line. The decrease seen along the left side of a speed line is due to the turbulence levels and length scale. As the mass flow decreases, there is increased turbulence in the wake because of increased flow separation near the fan trailing edge on the suction side.

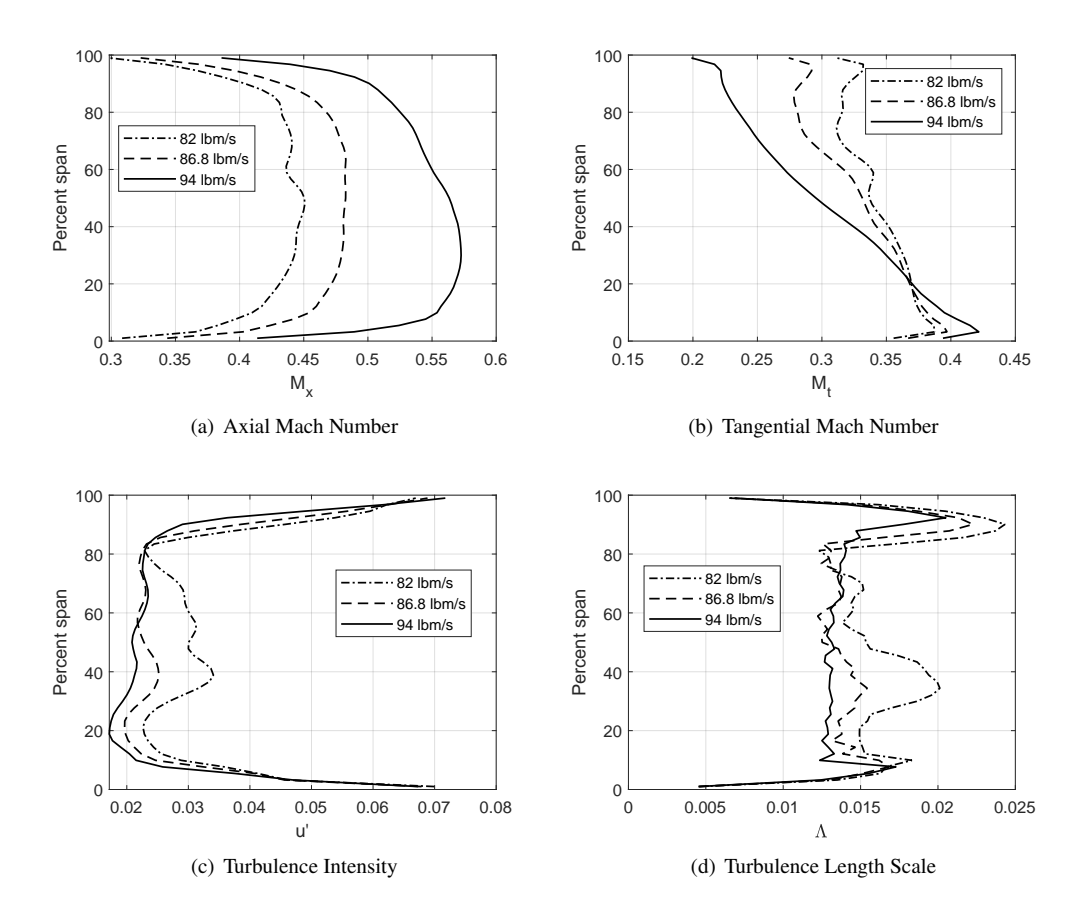


Fig. 10 Inputs for SDT cutback hot shape fan geometry at cutback fan speed, 87.5% or 11075 RPM.

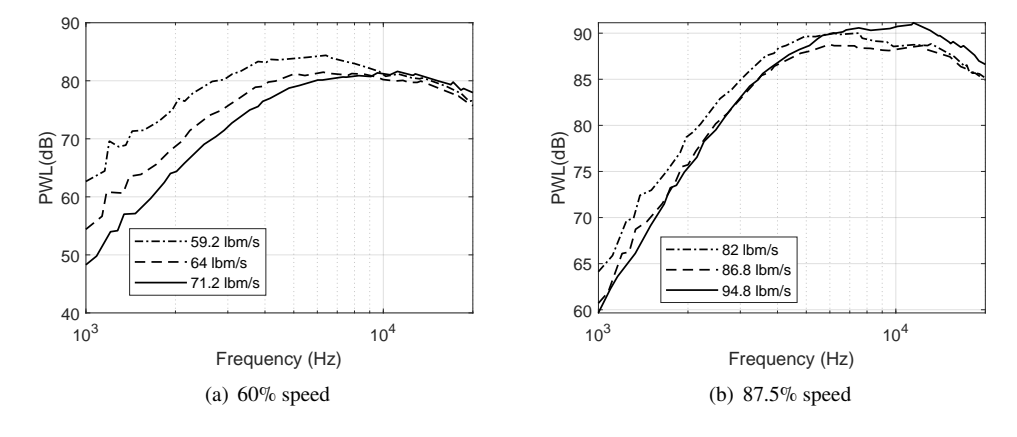


Fig. 11 Effect of mass flow rate on PWL prediction using SDT cutback hot geometry at two fan speeds.

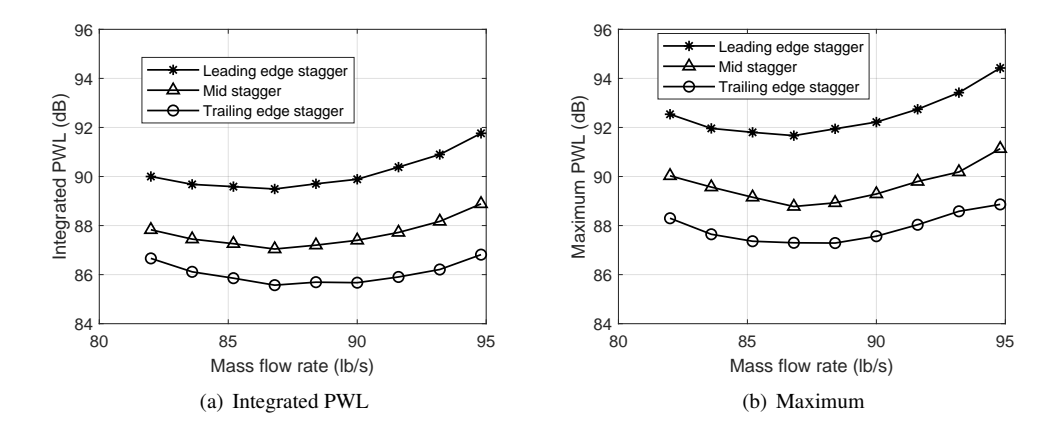


Fig. 12 Effect of stagger angle selection and mass flow rate on acoustic metrics. SDT cutback hot geometry at cutback fan speed.

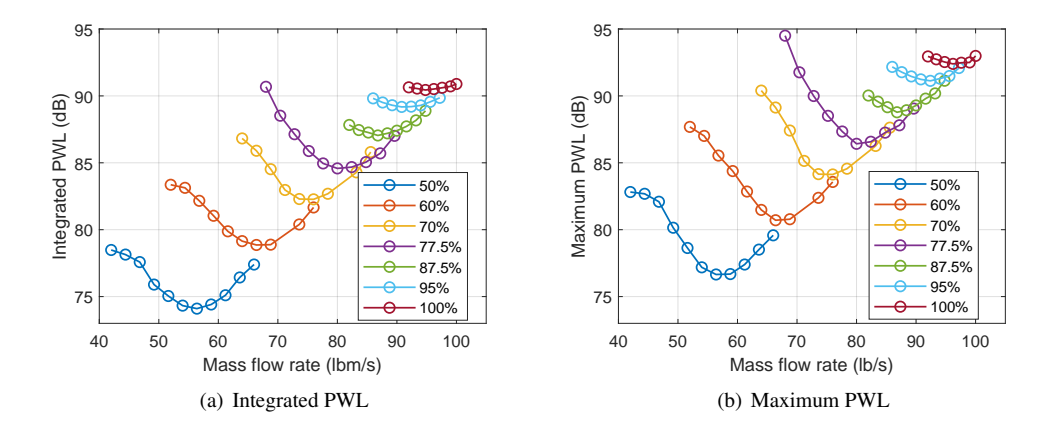


Fig. 13 Acoustic metrics for all speed lines and mass flows. SDT cutback hot geometry. Left: Integrated PWL. Right: Maximum PWL.

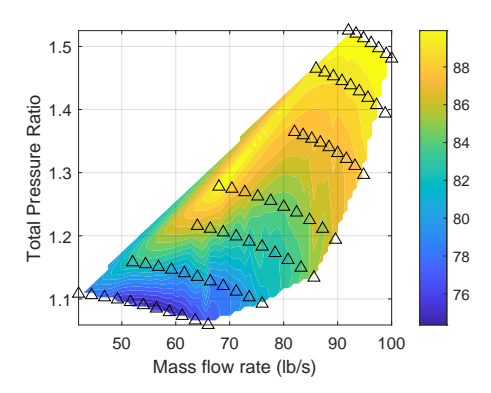


Fig. 14 Performance map with contour map of integrated PWL for cutback hot rotor geometry. Contour map values are in dB.

### B. Fan geometry

It has already been discussed that there are four geometries related to the SDT. In the past, each was used for exactly the case of interest, e.g. cutback hot was used when the noise from the cutback case was computed. However, access to the four geometries provides an opportunity to investigate whether the geometry differences would lead to different noise outcomes. As such, each geometry was used at two SDT fan speeds and multiple mass flows. The fan performance maps indicate that there are slight differences in performance as seen in Fig. 15. Still, the different fan geometries lead to almost no difference in the noise as shown in Figs. 16-17. Any difference that does arise is not linkable to the fan performance difference but instead to the increased turbulence at the lower mass flow where the trailing edge separation is increased. Fig. 18 shows the suction side boundary layer thickness at a fixed location just upstream of the trailing edge for each of the cases shown in Figs. 1617. The largest difference across geometries is seen at the lowest fan speed and lowest mass flow. Then, at the cutback fan speed and lower mass flow, the boundary layer for the approach hot geometry is smaller near midspan than the other three geometry cases. This leads to the slight difference seen in the spectra for these cases. The main takeaway is that the acoustic spectrum is not that sensitive to cold vs hot fan geometry. Therefore, the cold geometry can be used to predict the noise accurately and this is beneficial because it takes effort to create a hot geometry computationally.

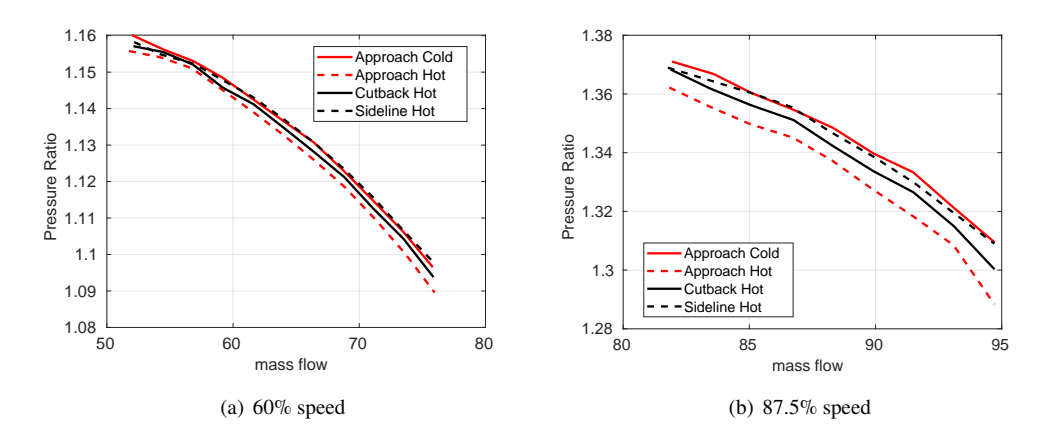


Fig. 15 Pressure ratio for 4 different fan geometries at 2 fan speeds.

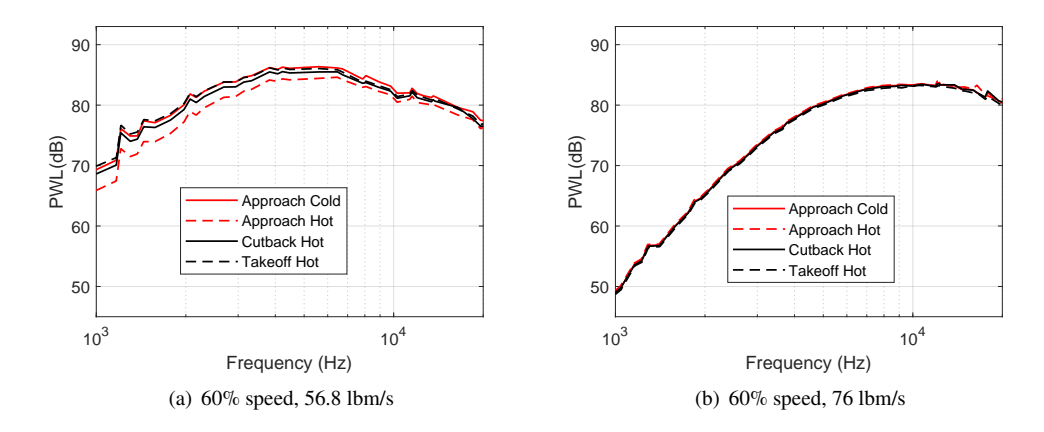


Fig. 16 Effect of using different fan geometry on predicted sound power level. 60% fan speed.

10

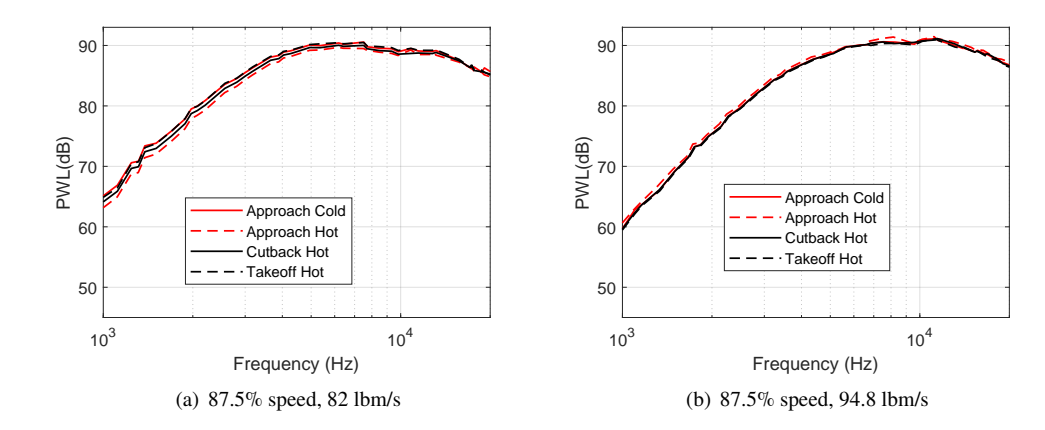


Fig. 17 Effect of using different fan geometry on predicted sound power level. 87.5% fan speed.

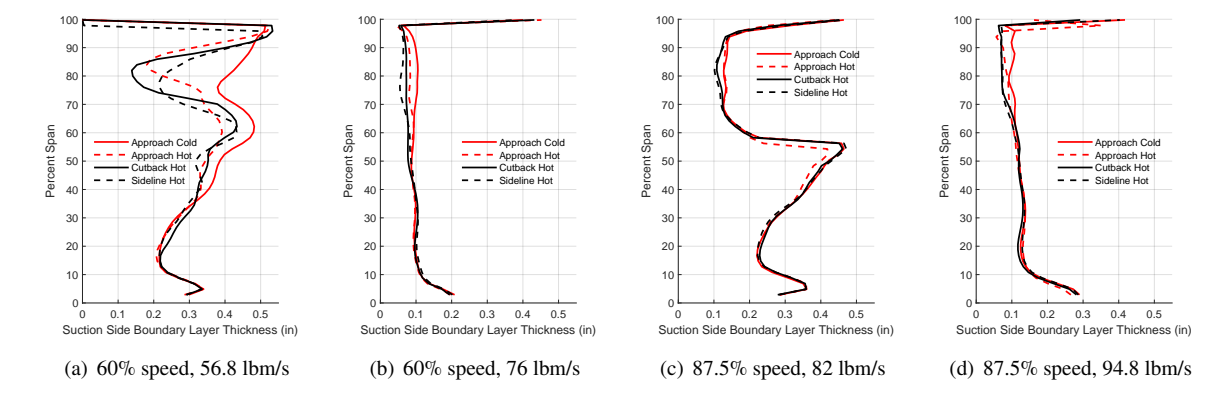


Fig. 18 Fan trailing edge suction side boundary layer thickness.

#### C. Interstage gap length

In this section, the effect of interstage gap length on sound power spectrum is investigated. Previously Behn and Tapken [7] compared the measured sound pressure level spectra between the ACAT1 long gap and short gap configurations. They described the short gap configuration spectrum as shifted to higher frequency as compared to long gap spectra and note slightly higher noise levels at high frequency and lower levels at low frequency. Blázquez and Corral [5] also show that the measured outlet  $\Delta PWL$  between short gap and long gap is negative at low frequency and positive at high frequency.

Here, the effect on broadband noise of placement of the SDT FEGV in relation to the fan is considered. The SDT approach case (61.7% fan speed, 58.3 lbm/s) with the baseline FEGV is modeled. The FEGV is moved from Station 2 to Station 1. The baseline FEGV trailing edge extends from 5.5 in to 11 in radially. The trailing edge radial extent is what is used to set the downstream annulus in the low-order noise calculation. If the FEGV is moved to Station 1, then its radial extent must be slightly increased as shown in Fig. 1. There are many ways to consider how the FEGV geometry could change if it were designed to be placed at the mid gap location. For this initial study, the FEGV is simply extended in the radial direction by aligning the actual FEGV and the mid-gap FEGV percent radius geometry specifications. At Station 1, the FEGV trailing edge must extend from 5.2 in to 11 in radially. This does not preserve the blockage induced by the FEGV; and it increases the assumed annular area of the downstream duct.

Differences then between the sound produced by the SDT FEGV in its original location and by a radially similar FEGV placed at Station 1 can be due to both the geometric change in the FEGV and downstream annulus and the inflow difference. The fan wake parameters for cutback hot geometry at 61.7% speed, 58.3 lbm/s at the two stations that provide the inflow conditions for the noise calculation are shown in Fig. 19. The three columns of figures refer to the experimental hotwire data, the results from the current rotor alone simulation, and previous results from a TSWIFT RANS simulation for the full fan stage [1].

The decrease in the annular geometry from Station 1 to Station 2 creates an increase in the axial Mach number at the farther downstream location. However, at Station 1 the circumferential velocity is higher. Together they give an almost unchanging streamwise mean flow between Stations 1 & 2. All of the methods for determining the FEGV inflow indicate that the turbulence intensity slightly decays and the length scale increases as the wake diffuses downstream of the fan. However, there is disagreement as to the magnitude of the changes. The TSWIFT calculation predicts much larger differences in the turbulence intensity and the length scale. The current simulations match the experimental data slightly better in this respect.

Fig. 20 shows the predicted noise for the SDT FEGV, placed at Station 2, and the radially similar FEGV placed at Station 1 based on inflow values taken from the hotwire data and the two RANS simulations. The hotwire result show the least difference between the noise from the two scenarios and the TSWIFT based results show the largest difference. All of the predictions show what Blázquez and Corral [5] found for the ACAT1: when the FEGV is at Station 1, the noise at low frequency is lower and at high frequency slightly higher.

In order to separate the effect of the change in the wake flow values and the change in FEGV and duct geometry, the following study was performed. The inflow values at Station 1 were used together with the FEGV at Station 2. That is, the flow inputs were characterized by percent radius and simply introduced in the calculation of the noise from the original FEGV. The results are shown as the dotted lines in Fig. 20. The dotted lines coincide with the results for the FEGV placed at Station 1. This indicates that the slight geometry differences needed for the FEGV to sit at Station 1 are not a significant factor.

To further check the trend with FEGV distance from the fan, the acoustic spectra were computed when the FEGV was placed halfway between the fan and Station 1 and then halfway between Stations 1 & 2. The clear progression of decreased acoustic power at the lower frequencies as distance between the FEGV and the fan decreases is seen in Fig. 20(b). Here this change is attributed to the length scale and the spectrum is characterized as slightly tilted. The increase in difference between the predicted spectrum based on the hotwire, rotor alone and then TSWIFT data can be seen to reflect the measured and predicted length scale difference from Station 1 to Station 2 in Fig. 19. Because the spectrum is tilted due to the length scale change, the overall integrated sound power level (between 600 and 20k Hz) remains nearly identical. This result implies that there is room in the design space to create a fan stage with a shorter interstage gap that would give similar broadband levels.

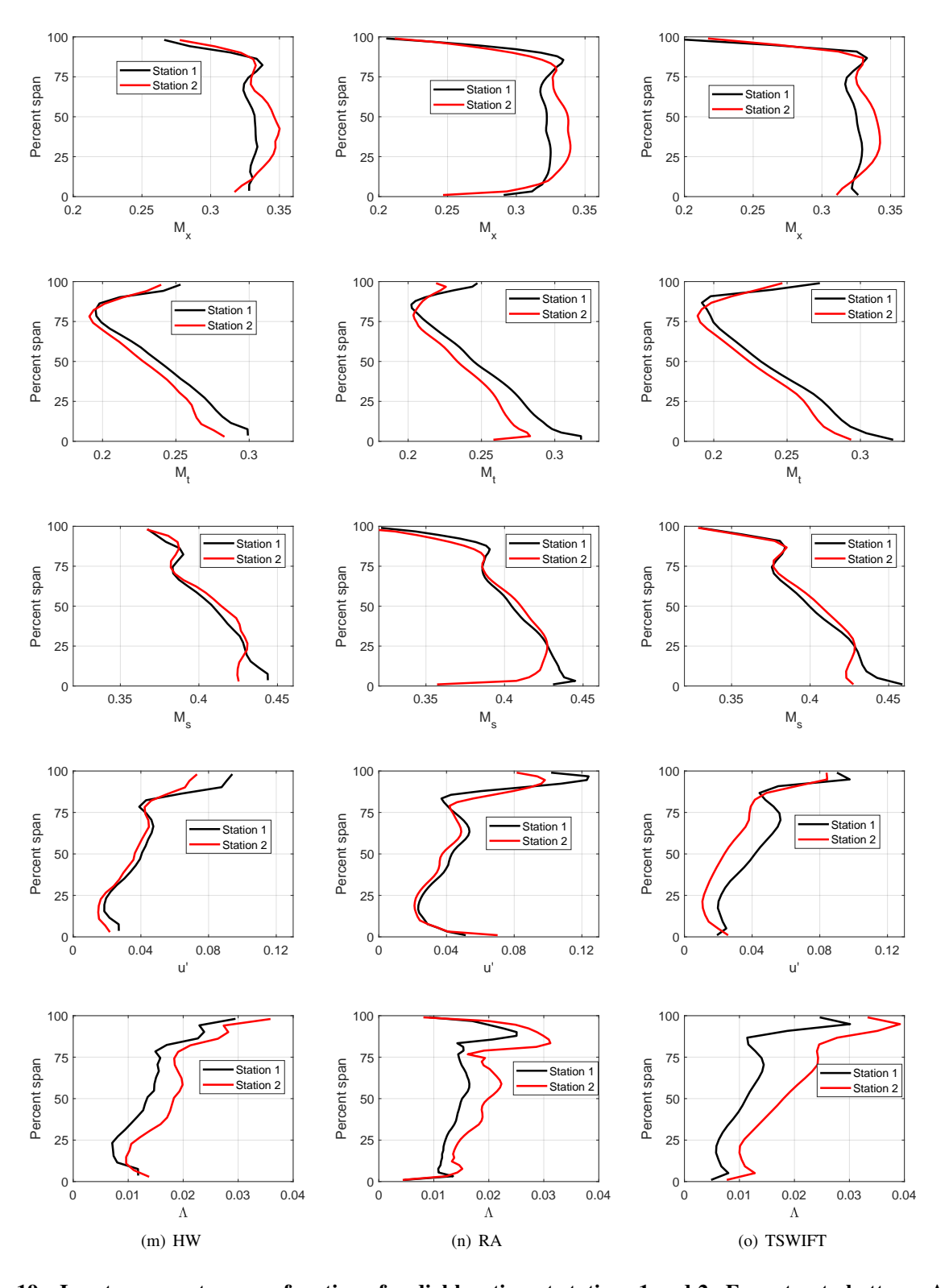


Fig. 19 Inputs parameters as a function of radial location at stations 1 and 2. From top to bottom: Axial Mach Number, Circumferential Mach number, Streamwise Mach number, turbulence intensity, longitudinal turbulence length scale. From left to right: HW: hotwire; RA: RANS rotor alone; TSWIFT: RANS rotor-stator.

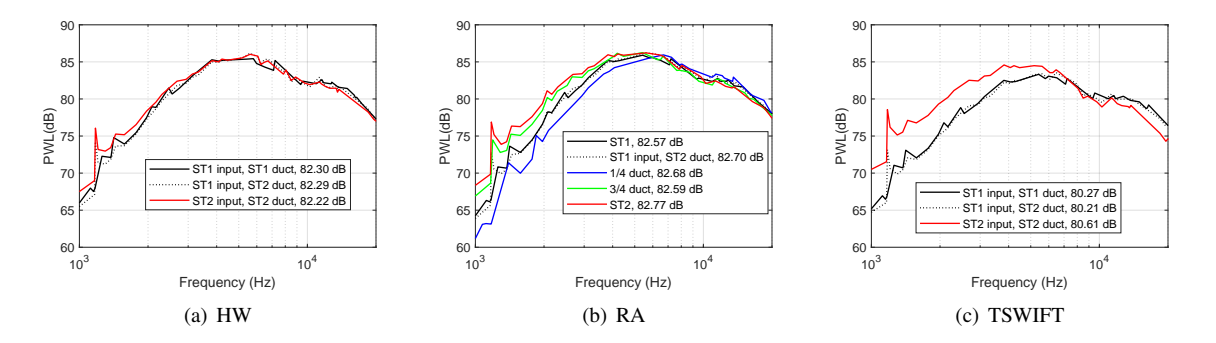


Fig. 20 Effect of moving FEGV further upstream. dB values are integrated PWL.

### D. Tip clearance

The effect of fan tip clearance for the SDT fan has been previously investigated through experiment by Hughes et al. [24]. They showed that the tip clearance has a clear effect on the fan alone noise with increased tip gap leading to increased broadband fan noise. However, because the fan-stage broadband interaction noise is much higher than the fan self noise, when the FEGV is included, the overall difference due to tip clearance becomes much smaller. Indeed the experimental results show barely 1 dB difference at any fan speed.

In our study, three tip clearances, 0.01", 0.02", and 0.03" are considered. The RANS simulations are performed using the cutback hot fan geometry at three speeds. The tip clearance gap is assumed to be constant across fan speeds because the blade deformation is not included. The main parameter affecting the acoustic prediction between the tip clearance cases is the turbulence length scale. Fig. 21 shows that reducing tip clearance reduces the turbulent length scale near the tip region, and the reduction is higher at higher speeds. Fig. 22 shows that tip clearance has very little impact on the acoustic spectrum at 61.7 % speed, while reducing tip clearance from 0.03" to 0.01" lowers the spectra by 2 to 3 dB at 87.5 % speed and 100 % speed at low frequency. The experimental data are contaminated by facility noise at low frequency so difference would not have been captured. Therefore, this prediction cannot be fully validated at this time. However, for realistic tip clearance differences, it is clear that the impact on the broadband noise is minimal.

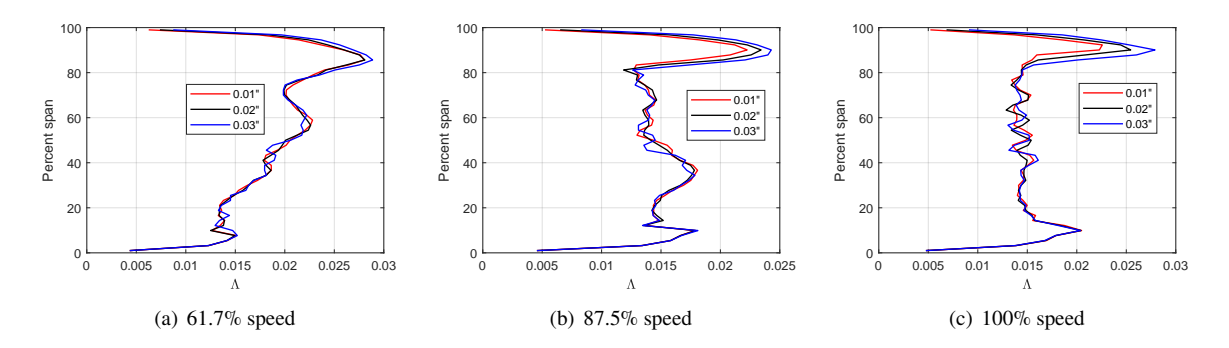


Fig. 21 Turbulence length scale inputs of three tip clearances at station 2.

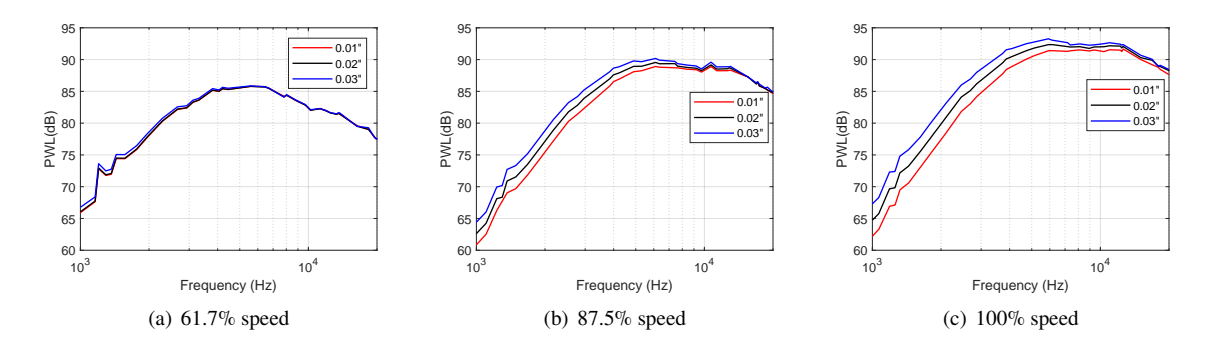


Fig. 22 Effect of tip clearance gap.

### VI. Conclusions

A low-order method for computing broadband interaction noise downstream of a fan stage has been used to consider some acoustic trends relevant to fan stage design. The method has a main limitation in that it can be relied on only for trends. It is shown that choice of model parameters specifically the selection of stagger angle significantly changes the results. However, once the model parameters are set, trends are captured well. Further, RANS is used to produce the fan wake inflow into the FEGV. Comparison between the RANS results and experimental data show that the RANS predictions are reasonable and capture the flow parameter trends for the most part. However, exact agreement between the RANS simulations and between the RANS and measured data is not demonstrated with differences in the length scale, particularly outboard, being the largest. This is unfortunate because of the major impact the length scale has on the acoustic spectrum. Still the predicted trends are all in the same direction with the magnitude of differences between cases being slightly differently depending on the source of the fan wake values used for input to the low-order method.

The method was used to consider the effect of slight fan geometry differences, mass flow variation and FEGV placement in the interstage. The difference in noise generated by the SDT cold and hot geometries was imperceptible at high mass flow rate and only 1-2dB different at low mass flow rate. At lower fan speed, there is an optimal mass flow rate which does not coincide exactly with the maximum efficiency point. Gap location of the FEGV is shown to not be a strong modifier of the overall broadband noise which enables shortening of the interstage gap if the tonal noise can be treated.

### **Acknowledgments**

This research was partially funded by the U.S. Federal Aviation Administration Office of Environment and Energy through ASCENT, the FAA Center of Excellence for Alternative Jet Fuels and the Environment, project 75 through FAA Award Number 13-C-AJFE-BU under the supervision of Christopher Dorbian. Any opinions, findings, conclusions or recommendations expressed in this material are those of the authors and do not necessarily reflect the views of the FAA. Other funding has come from RTRC and BU Mechanical Engineering Department. The development of the low-order acoustic method was funded through the Ohio Aerospace Institute on a grant from the AeroAcoustics Research Constortium.

### References

- [1] Grace, S., "Fan Broadband Interaction Noise Modeling Using a Low-Order Method," *Journal of Sound and Vibration*, Vol. 346, 2015, pp. 402–423.
- [2] Guérin, S., Kissner, C., Seeler, P., Blázquez, R., Carrasco Laraña, P., Laborderie, H., Lewis, D., Chaitanya, P., Polacsek, C., and Thisse, J., "ACAT1 Benchmark of RANS-Informed Analytical Methods for Fan Broadband Noise Prediction: Part II—Influence of the Acoustic Models," *Acoustics*, Vol. 2, 2020, pp. 617–649.
- [3] Cheong, C., Joseph, P., and Lee, S., "High frequency formulation for the acoustic power spectrum due to cascade-turbulence interaction," *Journal of the Acoustics Society of America*, Vol. 119, No. 1, 2006, pp. 108–122.

- [4] Posson, H., Moreau, S., and Roger, M., "Broadband noise prediction of fan outlet guide vane using a cascade response function," *Journal of Sound and Vibration*, Vol. 330, 2011, pp. 6153–6183.
- [5] Blázquez Navarro, R., and Corral, R., "Prediction of Fan Acoustic Blockage on Fan/Outlet Guide Vane Broadband Interaction Noise Using Efficient Frequency Domain Linearised Navier-Stokes Solvers," *Journal of Sound and Vibration*, Vol. 500, 2021, p. 116033. doi:10.1016/j.jsv.2021.116033.
- [6] Nallasamy, M., and Envia, E., "Computation of rotor wake turbulence noise," *Journal of Sound and Vibration*, Vol. 282, 2005, pp. 649–678.
- [7] Behn, M., and Tapken, U., "Investigation of Sound Generation and Transmission Effects Through the ACAT1 Fan Stage using Compressed Sensing-based Mode Analysis," AIAA Paper No. 2019-2502, 2019. doi:10.2514/6.2019-2502.
- [8] Goldstein, M. E., Aeroacoustics, McGraw-Hill International Book Co., New York, etc., 1976, p. 222.
- [9] Ventres, C., Theobald, M. A., and Mark, W. D., "Turbofan Noise Generation Volume 1: Analysis," Tech. Rep. CR-167952, NASA, July 1982.
- [10] Atassi, H. M., and Hamad, G., "Sound Generated in a Cascade by Three-Dimensional Disturbances Convected in a Subsonic Flow," AIAA Paper No. 81-2046, 1981, pp. 1–13.
- [11] Grace, S., "Further Investigations into a Low-Order Model of Fan Broadband Noise," *AIAA Paper No. AIAA 2015-3283*, 2015, pp. 1–15.
- [12] Ni, R. H., "A Multiple-Grid Scheme for Solving the Euler Equations," AIAA Journal, Vol. 20, No. 11, 1982, pp. 1565–1571.
- [13] Wilcox, D. C., Turbulence modeling for CFD, DCW industries, Canada, 1998.
- [14] Winkler, J., Reimann, C. A., Reba, R. A., and Gilson, J., "Turbofan Inlet Distortion Noise Prediction with a Hybrid CFD-CAA Approach," AIAA Paper No. 2014-3102, 2014.
- [15] Winkler, J., Reimann, C. A., Gumke, C. D., Ali, A. A., and Reba, R. A., "Inlet and Aft Tonal Noise Predictions of a Full-Scale Turbofan Engine with Bifurcation and Inlet Distortion," AIAA Paper No. 2017-3034, 2017.
- [16] Prasad, A., and Prasad, D., "Unsteady Aerodynamics and Aeroacoustics of a High-Bypass Ratio Fan Stage," *Transactions of the ASME*, Vol. 127, 2005, pp. 64–75.
- [17] Giles, M., "Non-reflecting boundary conditions for Euler equation calculations," AIAA Journal, Vol. 28, 1988, pp. 2050–2058
- [18] Pope, S. B., Turbulent Flows, Cambridge University Press, Cambridge, UK, 2000.
- [19] Maunus, J., Grace, S. M., Sondak, D. L., and Yakhot, V., "Characteristics of Turbulence in a Turbofan Stage," *Journal of Turbomachinery*, Vol. 135, No. 2, 2013, pp. 021024–1–10.
- [20] Hughes, C., Jeracki, R., Woodward, R., and Miller, C., "Fan Noise Source Diagnostic Test: Rotor Alone Aerodynamic Performance Results," *AIAA Paper No.* 2002-2426, 2005. doi:10.2514/6.2002-2426.
- [21] Hanson, D. B., and Horan, K. P., "Turbulence/Cascade Interaction Spectra of Inflow, Cascade Response, and Noise," AIAA Paper No. 98-2319, 1998, pp. 688–698. doi: 10.2514/6.1998-2319.
- [22] Hughes, C., Podboy, G. G., Woodward, R. P., and Jeracki, R. J., "The Effect of Bypass Nozzle Exit Area on Fan Aerodynamic Performance and Noise in a Model Turbofan Simulator," Tech. Rep. TM-2013-214029, NASA, 2013.
- [23] Atassi, H. M., and Logue, M. M., "Effect of Turbulence Structure on Broadband Fan Noise," AIAA Paper No. 2008-2842, 2008, pp. 1–14. doi:10.2514/6.2008-2842.
- [24] Hughes, C., Woodward, R., and Podboy, G., "Effect of tip clearance on fan noise and aerodynamic performance," AIAA Paper No. 2005-2875, 2005. doi:10.2514/6.2005-2875.